Sedimentary Geology xxx (2017) xxx–xxx

Contents lists available at ScienceDirect

Sedimentary Geology

journal homepage: www.elsevier.com/locate/sedgeo

Geochemistry of Lower Devonian terrigenous sedimentary rocks from the Belgian Ardenne: Source proxy and paleogeographic reconstruction

Jean-Clair Duchesne [a,*], Philippe Meus [b], Frédéric Boulvain [c]

[a] Department of Geology, Laboratory of Petrology, Geochemistry and Petrophysics, University of Liège, Quartier Agora, B20, allée du Six-Août, 12, 4000 Liège, Belgium
[b] Aquapole, University of Liege, Quartier Polytech 1, allée de la Découverte, 4000 Liège, Belgium
[c] Department of Geology, Sedimentary Petrology, University of Liège, Quartier Agora, B20, allée du Six-Août, 12, 4000 Liège, Belgium

ARTICLE INFO

Article history:
Received 10 December 2016
Received in revised form 8 November 2017
Accepted 12 November 2017
Available online xxxx

Keywords:
Lochkovian
Pragian
Emsian
Sedimentary petrology
Metasomatic processes
Postdepositional processes

ABSTRACT

Major and trace element (Rb, Sr, Ba, Zr, Ni, V, Zn, Cr, Y, Ce) compositions are studied in Lower Devonian terrigenous sediments from the Dinant Synclinorium and Ardenne Anticline (Belgian Ardenne). Five cross sections encompassing 148 samples in 19 formations have been studied. In the conventional [Al_2O_3 + Fe_2O_3-K_2O-Na_2O]–[K_2O]–[FeO + MgO] triangle, the rock compositions plot on the illite–chlorite tie line. This suggests that (1) the mineral association has reached equilibrium in the pressure and temperature range of the postdepositional evolution of the sediments; (2) the chemical system was open and K was a mobile component. Although the original composition of the sediment was modified, the AAFM = Al_2O_3/Al_2O_3 + FeOt + MgO parameter that reflects the illite-chlorite proportions can be used as a proxy of the source composition. A principal component analysis of the major and trace element compositions permits to define the behaviour of various elements currently used as proxies of various processes. Noteworthy it is shown that Ti, V and part of Cr are correlated with the illite proportion, and part of Cr, together with Zr, with resistate minerals such as quartz, chromite and zircon. The evolution with stratigraphic age in the 5 cross sections of the AAFM proxy reveals that there is a major change in the northern part of the Ardenne Anticline at the limit between the Mirwart Formation and younger formations, corresponding approximately to the Lochkovian to Pragian transition. There is a clear shift from an aluminium-rich source to a more conventional chlorite-rich source. In the paleogeographic evolution of this region the only possible source of the aluminium-rich sediment is the Rocroi Massif. Our results confirm sedimentological and palynological evidence that a "Rocroi Island" existed in the Lochkovian Sea. A decrease in Zr concentrations with distance to the Rocroi Massif also supports this hypothesis. The stratigraphic evolution of several parameters shows local variations that can be attributed to variable streams and depositional conditions in an alluvial deltaic or shallow sea environment.

1. Introduction

In fine-grained siliciclastic rocks, the mineralogy of source rocks and the weathering conditions largely determine the composition of the detrital flux to the sedimentary basin. These signals are of the utmost importance to reconstruct the paleogeography and the paleoenvironment at the time of deposition. These signals, however, have been considerably modified by weathering and reverse weathering reactions during postdepositional processes (see the review by Milliken, 2013). To which extent the compositions of siliciclastic rocks are still significant to reconstruct their source is one of the main concerns of the present paper. On the basis of whole-rock analyses of shales and slates from Belgian Lower Devonian rocks, it will be shown that their mineralogy basically consists of quartz, illite and chlorite, an assemblage resulting from a chemically open system evolution of detrital clay minerals. It follows that a new proxy based on the proportions of illite and chlorite can be proposed to characterize the detrital flux and the source rocks. A principal component analysis of the major and trace elements will help to understand the behaviour of various elements that are currently used as proxies (see the review by Sageman and Lyons, 2013) in postdepositional processes. In the northern part of the Ardenne Anticline there is evidence that a drastic change in source-rock compositions took place close to the Lochkovian-Pragian transition from aluminium-rich material to more common chlorite-rich one. The Rocroi Massif is the likely temporary source of the aluminium-rich material.

2. The Lower Devonian in the Ardenne

In the Belgian Ardenne Lower Devonian (Lochkovian, Pragian and Emsian) formations outcrop in the northern part of the Dinant Synclinorium and in the Ardenne Anticline (Fig. 1). They are made up of detrital sediments, essentially silts and pelites, with a total thickness of ~4 km in the Ardenne Anticline. They lie unconformably on the

* Corresponding author.
E-mail address: jc.duchesne@ulg.ac.be (J.-C. Duchesne).

https://doi.org/10.1016/j.sedgeo.2017.11.008
0037-0738/

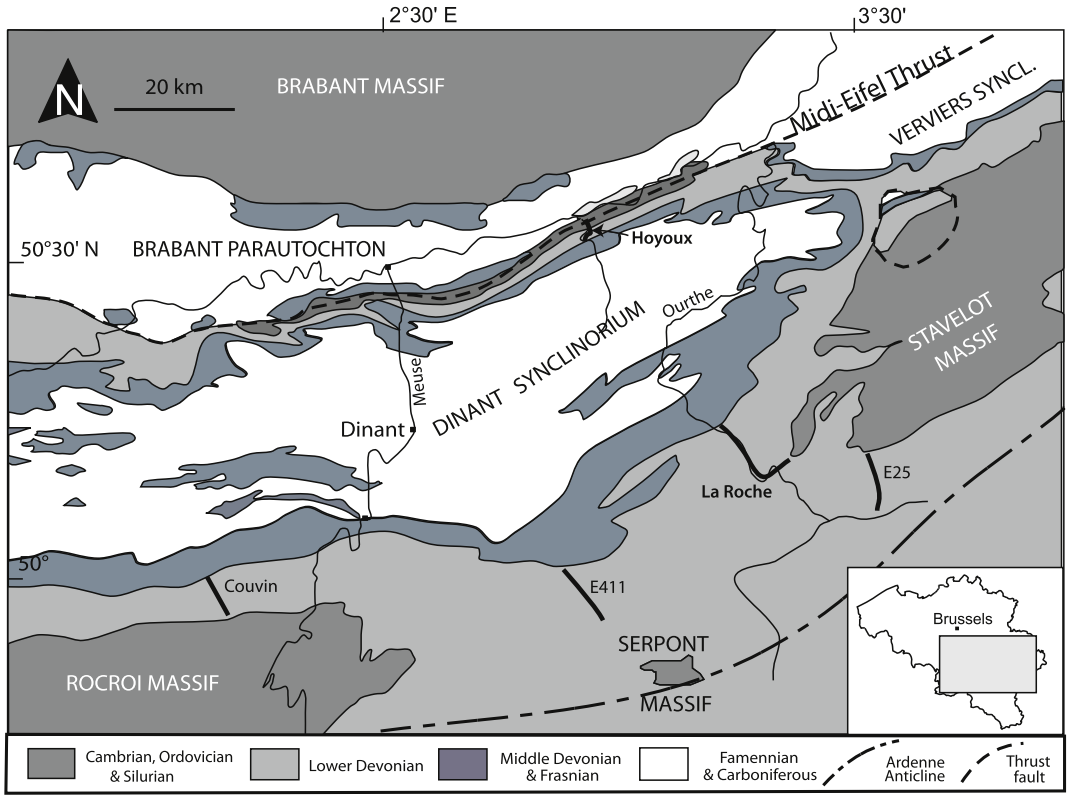

Fig. 1. Schematic geological map of the Dinant Synclinorium and Ardenne Anticline areas with location of the 5 cross sections in Lower Devonian rocks studied in this work.

Cambro-Ordovician of the Caledonian basement that outcrops namely in the Stavelot and Rocroi Massifs. The domain was affected by the Variscan orogeny that determined a progressive southward increase in burial metamorphism centred on the Ardenne Anticline (Beugnies, 1986) and culminating at 500 °C and 3–4 kbar (Fielitz and Mansy, 1999). The lower Devonian essentially made up of terrigenous sediments (sandstones, siltstones, shales and slates) has been divided in a number of lithostratigraphic units or formations (Bultynck and Dejonghe, 2001). They were deposited in an alluvial and deltaic environment (Lochkovian) (Stets and Schäfer, 2002) passing along a N-S transect to a tidal flat or shallow to open marine environment (Pragian) (Goemaere and Dejonghe, 2005; Stets and Schäfer, 2009) and again to a shallower environment with local carbonate deposits (Emsian).

The Lower Devonian basin was fed by terrigenous detritus coming from several sources. To the north the Brabant massif, part of the Old Red Continent, is universally considered as the main source of sediments in the Rhenohercynian basin, north-east of the studied region (Stets and Schäfer, 2002, 2009), as well as, since Fourmarier (Fourmarier, 1931), in the Ardenne Devonian basin. The Mid-German High is a second possible source of sediments. Located south of the area, it was emerged during Lochkovian and Pragian times and subsided only in early Emsian (Ziegler, 1990; Franke, 2000; Stets and Schäfer, 2009). The Rocroi Massif is another potential source. In the formation that unconformably lies on it, the pebble fabric in alluvial conglomerates suggests transport in high-density currents in streams centrifugally arranged perpendicular to the limits of the massif (Meilliez, 1984) This implies that the massif was an island in the Lochkovian Sea. Steemans (1989) also suggests a brief existence of the "Rocroi Island" at the beginning of Lochkovian times on the basis of reworked acritarchs from Cambrian to Ordovician ages in the Willerzie borehole close to the Rocroi massif. The influence of this source was however restricted to the neighbourhood of the island. The Stavelot Massif existed as an island in the Early Devonian sea and thus could be a source of detrital material in the Marteau Formation that corresponds to the main part of the Lochkovian (Boulvain and Pingot, 2016). It is also admitted that the Stavelot Massif emerged again at the end of Emsian times (Colbeaux et al., 1977). More details on the paleogeography of the Lower Devonian Basin are available in Boulvain and Vandenberghe (2017).

3. Methods of investigation

We have investigated the whole-rock compositions in several cross sections in Lower Devonian rocks (Meus, 1984; Wilmart et al., 1984) (Fig. 1). The cross sections have been chosen because they are representative of the stratigraphic succession of formations and of their lateral variations. The availability of outcrops has determined the sampling strategy and several samples per formation have been collected when possible. The first cross section (15 samples) extends southwards from Couvin in the Eau Noire River and Pernelle brook towards the contact with the Rocroi Massif (Fig. S1 in Supplementary data). More to the east, 19 samples were collected in boreholes east of Wellin along the E411 motorway (Fig. S2 in Supplementary data). Further east, the La Roche cross section (39 samples) is along the Ourthe River from Hampteau to La Roche-en-Ardenne and on the road from the later locality to Samrée (Fig. S3 in Supplementary data). The fourth cross section extends north of Houffalize in which 22 samples were collected in boreholes along the E25 motorway (Fig. S4 in Supplementary data). In the northern part of the Dinant Synclinorium a series of 53 samples along the Hoyoux River has also been studied (Fig. S5 in Supplementary data). Based on illite crystallinity (Fielitz and Mansy, 1999), the Hoyoux, Couvin and E411 rocks have been affected by anchizone metamorphism,

Please cite this article as: Duchesne, J.-C., et al., Geochemistry of Lower Devonian terrigenous sedimentary rocks from the Belgian Ardenne: Source proxy and paleogeographic reconstruction, Sedimentary Geology (2017), https://doi.org/10.1016/j.sedgeo.2017.11.008

Table 1
Concise description of the Lower Devonian formations.
(After Boulvain and Pingot (2016).)

A. Northern border of the Ardenne Anticline
Saint Joseph (STJ): 40 m?: Grey shales and siltites with layers/beds of fossiliferous limestones
Hampteau (HAM): 500–1000 m: Coarse-grained sandstones and conglomerates associated with shale and siltite beds
Chooz (CHO): 600–800 m: Reddish shales and siltites containing piles of sandstone beds
Pesche (PES): 700–800 m; Shales and siltites micaceous and nodular; rich in fossils
Jupille (JUP): 150–600 m: Piles of greyish sandstone beds in dark blue slates
La Roche (LAR): 350–800 m: Mainly dark blue slates or shales with accessory beds of siltites argillaceous sandstones or quartzites
Villé (VIL): 250–300 m: Slates with dm-thick beds of grey blue argillaceous sandstones and siltites
Mirwart (MIR): 300–700 m: Dark blue slates, shales and siltites interbedded with m-thick beds of light-coloured quartzites with undulating bedding
Saint Hubert (STH): 400–700 m: Green shales and siltites with rare thick greyish quartzitic lenticular beds
Oignies (OIG): 700–1200 m: Reddish slates with sandstone beds, locally micaceous, argillaceous or quartzitic
Mondrepuis (MOD): 0–250 m: Grey blue shales and slates

B. Northern border of the Dinant Synclinorium
Marteau (MAR): 100–150 m: red and green shales with lenticular beds of grey sandstones
Nonceveux (NON): ~100 m: series of greyish sandstones evolving towards maroon shales and slates
Solière (SOL): ~100 m: grey blue shales and siltites
Acoz: 50–400 m: maroon sandstones and siltites
Wépion (WEP): 200–400 m; grey-blue to greenish sandstones and quartzite with intercalations (?) of pelitic rocks

the La Roche section by conditions at the limit between anchizone and epizone (*c.* 300 °C) and the E25 cross section by epizonal conditions.

The samples belong to various formations defined on the geological maps (Marion and Barchy, 1999; Dejonghe and Hance, 2001; Dejonghe, 2008; Dumoulin and Blockmans, 2013a, b) and briefly described in Table 1 and Figs. 2 and 3. Fine-grained rocks (shales, siltites) were privileged in the sampling.

3.1. Analytical methods

The samples were crushed in agate mortars and analysed by XRF on a CGR Alpha-2020 semi-automatic spectrometer. The major elements (except Na) were analysed after calcination at 1000 °C for 4 h on Li tetraborate glass discs (Spectroflux Johnson Matthey) following the method of Norrish and Hutton (1969) with analytical

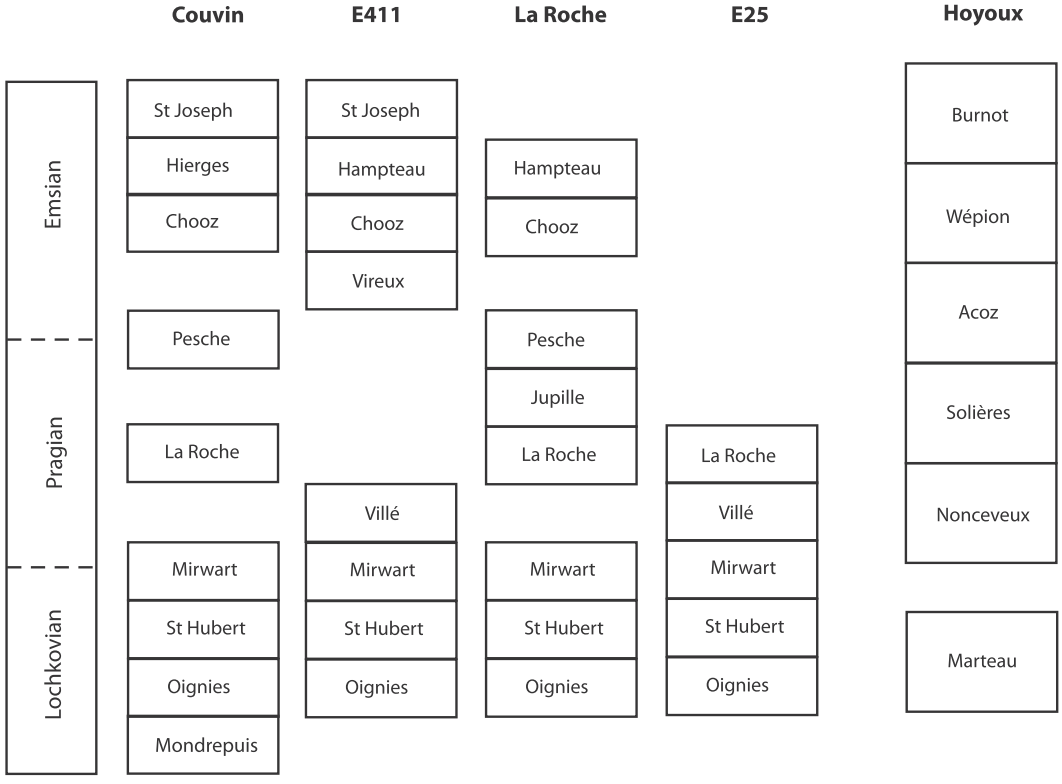

Fig. 2. The Lower Devonian lithostratigraphic units or formations occurring in the cross sections studied in this work (after Bultynck et al., 1991; Dejonghe and Hance, 2001; Dejonghe, 2008; Boulvain and Pingot, 2016). Not all formations may be present in a cross section due to stratigraphic hiatus or lack of outcrops.

Please cite this article as: Duchesne, J.-C., et al., Geochemistry of Lower Devonian terrigenous sedimentary rocks from the Belgian Ardenne: Source proxy and paleogeographic reconstruction, Sedimentary Geology (2017), https://doi.org/10.1016/j.sedgeo.2017.11.008

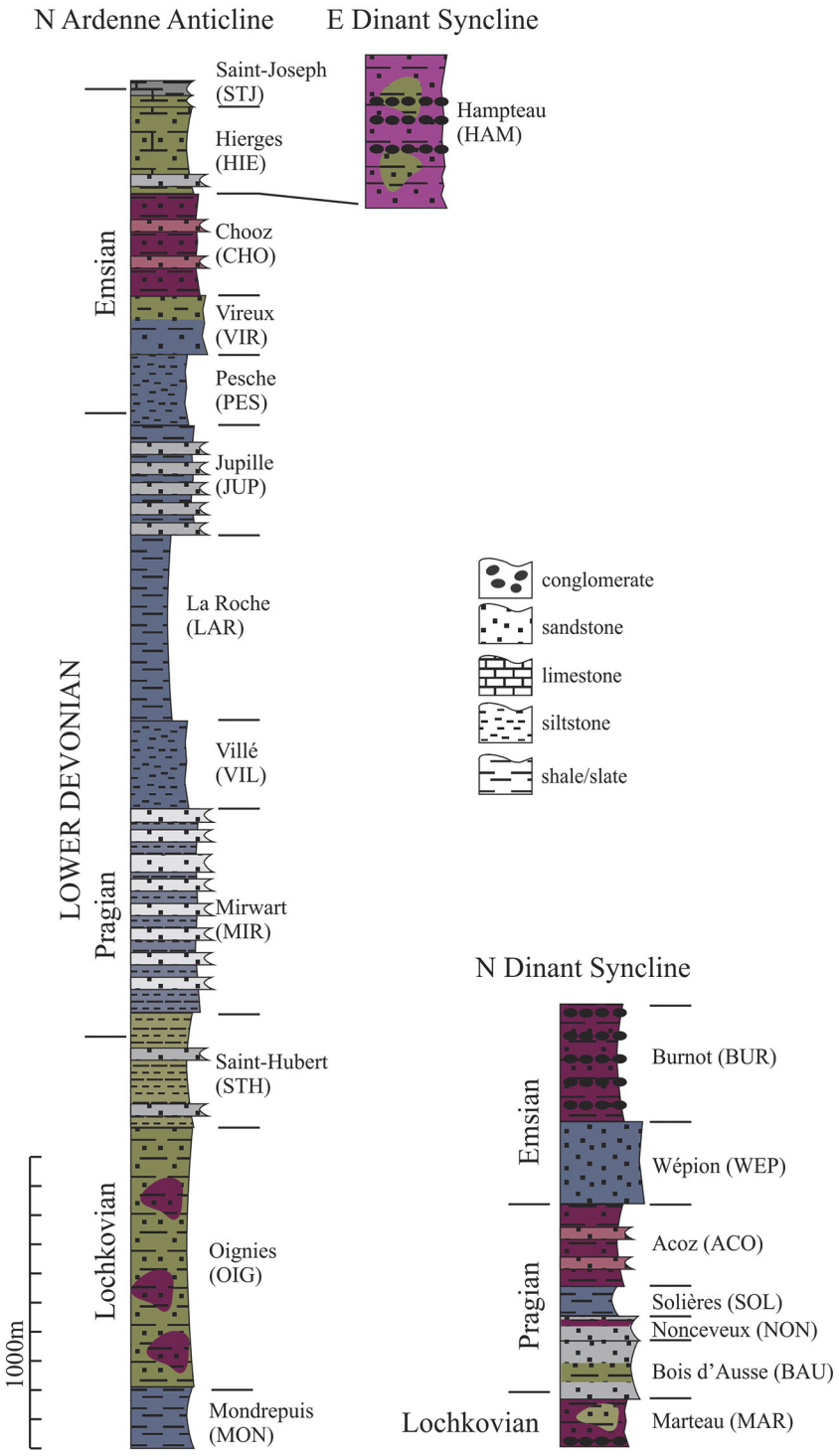

Fig. 3. Schematic synthetic logs of the Lower Devonian formations in the Northern border of the Ardenne Anticline, and the Northern and Eastern borders of the Dinant Syncline. Thicknesses and facies are speculative and fluctuate due to important lateral variations in the sedimentary and tectonic settings.
(After Godefroid et al. (1994).)

conditions described in Bologne and Duchesne (1991). Calibration was performed with international reference samples (GA, GH, DRN, BR) and three Belgian sedimentary rock reference materials (AWI, SBO, PRI) (Roelandts and Duchesne, 1988, 1994). Trace elements were measured on pressed pellets. Sr, Rb, Zr and Y were corrected for matrix effects by Compton peak monitoring and Zn, Ni and Cr by background intensity monitoring. Reference materials with similar compositions were simply used without matrix correction for V, Ba and Ce. Na was also measured on pressed pellets with absorption coefficients used in matrix corrections calculated with reference materials. In the La Roche cross section, FeO was measured by titration with $K_2Cr_2O_7$.

Please cite this article as: Duchesne, J.-C., et al., Geochemistry of Lower Devonian terrigenous sedimentary rocks from the Belgian Ardenne: Source proxy and paleogeographic reconstruction, Sedimentary Geology (2017), https://doi.org/10.1016/j.sedgeo.2017.11.008

3.2. Petrography and composition of the sediments

Thin sections of all the samples were studied under the microscope. The sample collection is monotonous. The rocks are made up of various proportions of quartz in a clay mineral matrix consisting in a very fine-grained mixture of sericite/illite and chlorite. Larger grains of chlorite occur locally as well as detrital flakes of muscovite/illite. Opaque minerals and zircon are common accessories. Details on the petrographic characteristics are given in Supplementary Tables S1 and S2.

We focus on the La Roche cross section that is representative of most Lower Devonian formations. The chemical compositions of 39 samples are reported in Table 2. In the geochemical classification of terrigenous sands and shales (Herron, 1988), whatever their belonging to the various formations defined in Table 1, most samples are shales forming a trend extending into wackes and litharenites. Two samples are arkose/subarkose, two others are close to the litharenite-sublitharenite limit and one sample is a clear litharenite (Fig. 4).

4. Results and discussion

4.1. The AKF diagram

In order to link the bulk composition of a rock with its mineralogy, we adopt the graphical representation introduced long ago by Eskola (1920) and extensively used in metamorphic petrology (e.g. Turner and Verhoogen, 1960; Verhoogen et al., 1970; Winkler, 1979; Bucher and Frey, 1994; Winter, 2001) and less often for phyllosilicate assemblage (e.g. Velde, 1983). To represent the composition of the minerals occurring in siliciclastic rocks, we need the concentrations in Si, Al, Fe^{3+}, Fe^{2+}, Mg, K and Na. The low amounts of Ti, Mn and P can be ignored and Ca can be neglected except in a few rocks where it occurs as calcite. Following geochemical affinities in the sedimentary environment (e.g. Al^{3+} and Fe^{3+}) or in mafic minerals (e.g. Fe^{2+} and Mg), the needed elements can be combined in 3 constituents plotted at the apexes of a triangle. In this AKF diagram the constituents expressed in moles are $A = Al_2O_3 + Fe_2O_3 - Na_2O - K_2O$; $K = K_2O$; $F = FeO + MgO$.

Fig. 5 illustrates the position of several common minerals in siliciclastic rocks. Note that quartz is not represented in the diagram but there is sufficient content in SiO_2 in the rock for quartz to always exist (it is considered "in excess") together with the minerals represented in the AKF diagram. It is also supposed that Na is combined in albite, an approximation quite acceptable considering the low average content of Na_2O (0.82%). H_2O, needed to build up clay minerals, is also considered as "in excess", which implies that a vapour phase was always present in the system during the postdepositional evolution.

The AKF constituents can be considered as the components of the Gibbs phase rule that expresses that, at equilibrium in a range of pressure and temperature, the maximum number of phases/minerals is equal to the number of components. Thus, in the AKF diagram, 3 phases at the apexes of a triangle form the equilibrium paragenesis of a rock whose composition plots within the triangle. For example in Fig. 5, the rock composition R plots inside the triangle illite-chlorite-kaolinite, which means that these phases + quartz + albite + vapour are in equilibrium in the sample.

4.2. Mobility of potassium

The compositions of the samples of Table 2 are plotted in the AKF diagram in Fig. 6. Interestingly all compositions are very close to a tie line between an illite and a chlorite instead of being inside a triangular area. This has several implications. First, illite and chlorite are in equilibrium or very close to equilibrium. This is not unexpected because in diagenetic processes it is well demonstrated that smectite is easily transformed in authigenic illite through the reaction smectite + K^+ + Al^{3+} = illite + Si^{4+} with the release of some Fe^{2+} and Mg^{2+} (e.g. Hower et al., 1976; Chamley, 1989; Milliken, 2013; Sageman and Lyons, 2013). The K and Al appear to be derived from the decomposition of K-feldspar and possibly of some mica, and the excess Si forms authigenic quartz. Associated with the formation of illite and the decomposition of K-feldspar is the formation of authigenic chlorite, as clearly shown for instance in a well of the Gulf Coast (Hower et al., 1976). This mineral is likely formed from magnesium and iron released by smectite. It is thus suggested that the total reaction is smectite + K-feldspar = illite + chlorite + quartz. Our data confirm the stability of the three minerals in the siliciclastic material.

Second, as shown in Fig. 5, the overall composition of a rock R reacts with K-feldspar to produce illite + chlorite (+quartz) and after the reaction rock R contains illite, chlorite and a third phase, kaolinite, in excess compared to the final products. In the present case, this phase in excess is absent. What is the meaning of this absence? This strongly suggests that the rock during diagenesis was not a chemically closed system at the scale of a hand specimen. The composition of the rock R has moved towards R′ which lies on the illite-chlorite tie line. This can be done by increasing its potassium content, either by decomposing K-feldspar, or by reacting with K^+ ions present in pore fluids. Note that some rocks could also lose potassium in this process: rock composition S, initially associating e.g. K-feldspar, chlorite and smectite, would move to S′ on the illite-chlorite join. Thus, the rocks will gain or lose potassium at the scale of the sample, but if the pore fluids could permit chemical exchange between the rocks, potassium could be redistributed between various rocks and the system at the scale of the basin could remain close. Evidence that a rock remains a chemically close system during diagenesis and burial metamorphism (except for some elements such as Ca) is still debated. Hower et al. (1976) in a study on core samples in a Gulf Coast well concluded that the "variations in the bulk chemical composition of the shale with depth show only minor change, except for a marked decrease in CaO" (concomitant with the decrease in calcite), but the authors recognized the difficulty to discriminate primary variations related to sorting and provenance from diagenetically induced variations. The same limitations in the approach were also considered by a number of authors (see the review by Milliken, 2013). Our data strongly suggest, however, that potassium metasomatism takes place in postdepositional processes of siliciclastic sediments.

4.3. A new source proxy

It is clear from Fig. 5 that diagenesis and potassium metasomatism bring drastic change in the mineralogy of the original sediments as well as chemical changes in the bulk composition. We nevertheless suggest that some characteristics of the source rocks are still preserved. Indeed, due to the potassium mobility, the shift of the initial compositions R or S towards R′ or S′ on the illite-chlorite tie line does not modify the initial A/F ratio. In other words, whatever the initial detrital mineral association in the original sediment, this ratio can be used as a proxy to the provenance. We propose to express the ratio as $AAFM = Al_2O_3/(Al_2O_3 + FeO_t + MgO)$ (mol%). A high value represents an aluminium-rich source (e.g. a kaolinite-rich source) and a low value a Fe- and Mg-rich one (e.g. a smectite and/or chlorite-rich source).

4.4. Revisiting some proxies

A statistical treatment of the analytical data has been applied in order to better understand the behaviour of some elements. The result of an R-mode principal component analysis (PCA) is graphically

Please cite this article as: Duchesne, J.-C., et al., Geochemistry of Lower Devonian terrigenous sedimentary rocks from the Belgian Ardenne: Source proxy and paleogeographic reconstruction, Sedimentary Geology (2017), https://doi.org/10.1016/j.sedgeo.2017.11.008

Table 2
Major and trace element composition of Lower Devonian terrigenous rocks from the La Roche cross section.

Formation	St Joseph		Hampteau			Chooz						Pesche							
Sample	L1-1	L1-2	L2	PM6	PM1	PM34	L15	PM13	L3-1	L3-2	L4	PM33	PM10	L5-1	L5-2	PM16	L6-1	L6-2	PM17
Major elements (%)																			
SiO_2	53.58	68.7	80.18	73.12	67.81	59.32	59.4	66.71	52.92	72.78	56.68	70.39	78.14	55.17	68.35	72.25	62.29	71.86	78.65
TiO_2	0.79	0.41	0.42	0.67	0.83	1.04	0.98	0.87	0.96	0.49	0.96	0.85	0.58	0.85	0.64	0.84	0.84	0.75	0.57
Al_2O_3	18.54	7.9	8.86	12.51	13.88	19.73	19.09	14.82	23.04	10.03	21.89	13.53	9.66	20.52	12.6	11.12	17	9.74	9.43
Fe_2O_3	4.19	1.27	2.31	2.81	5.11	3.18	7.92	5.75	8.70	1.75	4.91	4.21	2.04	4.49	1.81	2.06	1.98	1.44	1.82
FeO	2.96	2.88	2.61	2.83	2.88	4.8	0.71	2.3	1.02	4.18	2.13	2.73	2.14	4.51	5.1	3.88	4.67	3.88	2.66
Fe_2O_3Tot	7.48	4.47	5.21	5.95	8.31	8.51	8.71	8.3	9.83	6.39	7.27	7.24	4.42	9.5	7.47	6.37	7.16	5.75	4.77
MnO	0.09	0.17	0.24	0.07	0.05	0.06	0.49	0.08	0.17	0.75	0.12	0.08	0.01	0.37	0.29	0.21	0.14	0.29	0.05
MgO	2.74	2.5	1.18	1.11	1.77	2.08	2.04	1.1	1.3	1.5	1.73	1.24	1.39	2.78	2.02	1.59	2.23	1.84	1.12
CaO	3.53	6.5	0.18	0.18	0.28	0.31	0.3	0.25	0.37	1.01	0.27	0.19	0.15	0.33	1.04	1.22	0.88	2.67	0.22
Na_2O	0.44	0.73	0.2	0.39	0.42	0.5	0.68	0.69	0.73	0.5	0.9	0.46	0.69	0.71	0.9	0.76	0.81	0.78	1.35
K_2O	4.21	1.32	1.86	2.5	2.72	4.14	3.57	2.45	4.43	1.33	4.09	2.37	1.52	4.25	1.84	1.7	3.25	1.62	1.26
P_2O5	0.04	0.11	0.02	0.1	0.13	0.14	0.12	0.14	0.21	0.07	0.18	0.14	0.03	0.11	0.09	0.11	0.06	0.08	0.11
PF	8.18	7.93	3.04	3.65	3.84	4.83	5.21	4.05	6.23	4.71	5.65	3.83	2.59	5.61	4.53	4.24	5.07	5.62	2.36
Total	99.29	100.42	101.10	99.94	99.72	100.13	100.51	99.21	100.08	99.10	99.51	100.02	98.94	99.70	99.21	99.98	99.22	100.57	99.60
Trace elements (ppm)																			
Ba	484	208	239	365	455	542	715	542	615	269	581	394	261	584	290	269	473	280	204
Ce	83	32	314	174	110	120	127	86	137	88	134	83	65	137	86	91	116	66	69
Cr	178	94	81	128	138	172	133	118	104	104	135	136	202	149	125	465	167	152	260
Ni	75	39	43	55	62	70	77	68	56	46	60	59	40	69	61	49	60	33	53
Rb	144	60	99	106	114	182	163	113	174	59	199	106	70	201	96	81	105	76	60
Sr	156	132	140	124	88	88	94	73	95	88	134	65	54	100	90	81	97	103	64
V	173	69	95	122	143	177	169	138	219	105	185	127	86	189	107	104	154	90	76
Y	25	36	56	31	32	32	33	32	19	26	26	33	24	36	30	43	21	34	25
Zn	83	77	35	75	106	131	114	120	101	125	109	88	57	103	109	111	93	108	101
Zr	168	158	209	211	310	201	210	286	133	184	181	289	375	172	255	544	250	484	385
AAFM	0.53	0.40	0.48	0.55	0.48	0.55	0.54	0.53	0.59	0.46	0.62	0.52	0.51	0.52	0.46	0.48	0.53	0.45	0.51
#Mg	0.42	0.53	0.31	0.27	0.30	0.33	0.32	0.21	0.21	0.32	0.32	0.25	0.38	0.37	0.35	0.33	0.38	0.39	0.32

Formation	Jupille	La Roche									Mirwart			St Hubert				Oignies		
Sample	PM18	L7-1	L7-2	PM28	L8	L9-1	L9-2	L9-3	L10-1	L10-2	L11	L12	PM32	PM30	PM22	L13-1	L13-2	PM29	PM23	PM24
Major elements (%)																				
SiO_2	78.53	61.25	56.38	67.54	82.37	61.57	59.93	59.5	61.43	82.51	94.46	64.14	63.13	60.83	87.05	67.55	67.87	66.55	87.66	64.86
TiO_2	0.54	0.84	0.91	0.83	0.29	0.89	0.89	1	0.92	0.47	0.31	0.91	0.92	1.16	0.47	0.91	0.89	1.03	0.47	0.96
Al_2O_3	8.31	17.75	20.3	15.12	6.07	17.76	18.19	19.32	17.81	5.74	3.36	17.93	17.97	22.36	7.52	17.77	17.28	19.19	7.05	15.52
Fe_2O_3	1.39	2.05	2.23	2.44									7.97	2.71	0.46	4.17	5.48	2.37	0.67	8.54
FeO	2.87	3.98	5.31	4.07									0.10	1.62	0.24	0.98	0.61	1.02	0.15	1.12
Fe_2O_3Tot	4.58	6.47	8.12	6.96	3.78	6.9	7.7	7.85	7.2	2.2	0.55	6.59	8.08	4.51	0.73	5.26	6.16	3.5	0.84	9.78
MnO	0.16	0.18	0.16	0.07	0.18	0.14	0.24	0.22	0.12	0.08	0.01	0.16	0.18	0.06	0.01	0.02	0.01	0.05	0.03	0.26
MgO	1.32	2.49	2.62	1.95	1.11	2.43	2.89	2.39	2.79	0.95	0.29	0.65	0.6	1.16	0.2	1.33	0.84	0.65	0.2	1.02
CaO	0.92	1.15	0.55	0.17	1.04	0.66	0.77	0.3	0.64	2.01	0.05	0.13	0.16	0.18	0.15	0.16	0.12	0.16	0.27	0.11
Na_2O	1.23	0.99	0.89	0.69	1.17	0.75	0.91	0.9	1.25	1.22	0.65	0.98	0.92	1.07	0.77	1.01	1.14	1.45	0.64	0.74
K_2O	1.18	3.76	4.28	2.91	0.79	3.52	3.46	3.75	3.31	0.89	0.31	3.83	3.59	4.56	1.06	3.71	3.48	3.46	1.2	3.16
P_2O5	0.11	0.04	0.09	0.12	0	0.08	0.1	0.13	0.1	0.04	0	0.11	0.13	0.11	0.06	0.03	0.02	0.12	0.16	0.05
PF	3.02	5.3	5.14	3.72	3.02	5.01	4.44	3.75	4.33	3.66	0.9	5.01	4.93	4.33	1.99	3.14	3.02	3.9	1.63	3.37
Total	99.58	99.78	98.86	99.63	99.82	99.71	99.52	99.11	99.90	99.77	100.89	100.44	100.60	100.15	99.98	100.78	100.76	99.95	100.13	99.71
Trace elements (ppm)																				
Ba	192	507	546	445	102	451	478	552	558	135	63	625	692	985	226	722	717	738	247	115
Ce	47	95	114	81	30	93	95	105	81	30	30	104	104	114	47	102	87	105	49	99
Cr	225	182	186	212	70	189	212	226	255	350	368	221	207	251	379	239	215	282	262	208
Ni	52	71	80	71	29	78	72	82	81	12	12	80	87	47	18	52	37	61	18	76
Rb	54	174	199	123	48	129	171	164	145	43	14	178	180	189	50	182	163	162	59	156
Sr	85	132	98	78	110	91	114	94	118	116	46	115	134	216	56	134	129	139	66	94
V	71	163	177	135	52	156	165	171	153	46	27	163	162	166	48	157	152	156	52	160
Y	25	18	26	28	12	17	23	25	23	9	14	29	26	25	18	27	31	25	14	32
Zn	58	112	110	107	32	104	87	93	103	12	12	82	107	84	18	46	30	58	23	82
Zr	305	175	173	268	115	167	219	282	244	486	199	264	205	208	253	244	259	231	262	331
AAFM	0.47	0.55	0.54	0.52	0.44	0.54	0.51	0.55	0.52	0.52	0.70	0.64	0.60	0.72	0.84	0.64	0.63	0.76	0.82	0.51
#Mg	0.36	0.43	0.39	0.36	0.37	0.41	0.43	0.38	0.43	0.46	0.51	0.16	0.13	0.34	0.35	0.33	0.21	0.27	0.32	0.17

Please cite this article as: Duchesne, J.-C., et al., Geochemistry of Lower Devonian terrigenous sedimentary rocks from the Belgian Ardenne: Source proxy and paleogeographic reconstruction, Sedimentary Geology (2017), https://doi.org/10.1016/j.sedgeo.2017.11.008

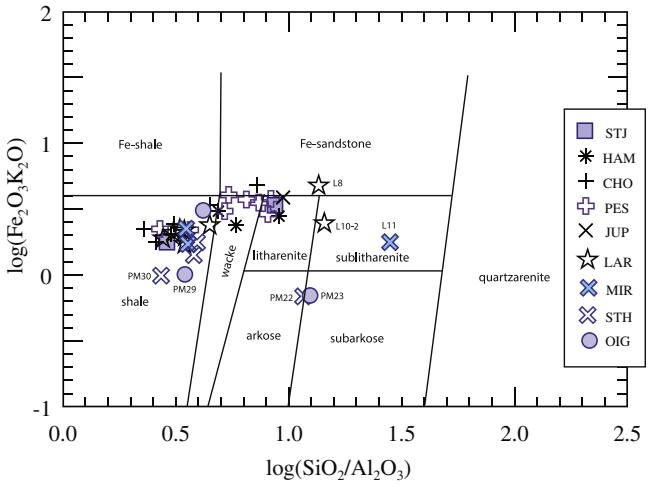

Fig. 4. Geochemical classification of the depositional rocks in the La Roche cross section following Herron (1988). Abbreviations of the formations names as in Fig. 3.

shown in Fig. 7. Five factors represent 80% of the total variance of the population. The first factor, positively loaded with Si, Zr and Cr and negatively correlated with a large group of elements, may be interpreted as a sorting factor or quartz-dilution factor. It represents the resistate minerals (quartz, zircon, chromite) relative to other detrital minerals. The second factor opposes the elements commonly found in illite (K, Rb, Al, and possibly Na) to those forming chlorite and carbonate (Fe, Mg, Ca). It can be compared to the illite/chlorite ratio defined above. The three other factors are difficult to decipher and mainly concern minor and trace elements. This PCA analysis throws some light on the behaviour of some elements. Ti appears correlated with illite in the first two factors, which suggests that it substitutes for Si or Al into the structural unit. It does not significantly occur in minerals such as ilmenite, commonly occurring with zircon and other resistate minerals in paleoplacers. We do not know exactly in which form Ti was present in the initial sediment, but it is very likely that it could be present in detrital clays. Chamley (1989) reports analyses of detrital illite, smectite and chlorite with average values of 0.54, 0.50 and 0.80% TiO_2, respectively. Vanadium and Cr have a variety of valence states and, in the literature (e.g. Sageman and Lyons, 2013), they are considered sensitive to variations in redox conditions, hence may characterize authigenic processes. In our PCA analysis, Cr is partly linked to the resistate minerals in factor F1, and to illite in factor F2. It could thus occur in the discharge partly as detrital chromite and partly as a trace element in clay minerals further redistributed in illite during diagenesis. Vanadium appears exclusively linked to K and Al in factor F1, thus pointing to its redistribution in illite. It thus seems that, in this particular case, V concentrations and at least part of Cr concentrations are not relevant indicators of redox variations in the depositional environment. The behaviour of REE elements (Ce and Y) remains enigmatic: Y is linked to chlorite in factor F2 and Ce and Y are negatively loading factor F3. This points to a complex behaviour of these elements in post-depositional processes (Ohr et al., 1994). Manganese appears closely linked to Fe and Mg in Factor F1 and thus its variations are expected to mirror those of chlorite. In the particular case of the Belgian Ardenne, the Mn concentrations might also indicate a possible influence of the Stavelot Massif as a source of material. The Stavelot Massif is indeed made up of Middle-Ordovician sedimentary rocks particularly rich in Mn (Kramm, 1973, 1976). In a survey of 31 rocks ranging in composition from 0.14 to 20.44 wt% MnO an average composition of 2.67 wt% MnO was reported (Bossiroy, 1984). It should be expected that detritus from these rocks would be much richer in MnO than average shales (PAAS = 0.11% MnO; Taylor and McLennan, 1985).

4.5. Stratigraphic evolution in the La Roche cross section

Variation with stratigraphic age of AAFM, #Mg (= MgO/(MgO + FeOt) (mol%) and Al/Ti ratios, together with concentrations of some characteristic elements Mn, Cr, V and Zr are shown on Fig. 8. It is interesting to note that the Oignies, Saint Hubert and Mirwart Formations (OSM) are characterized by high values of the AAFM

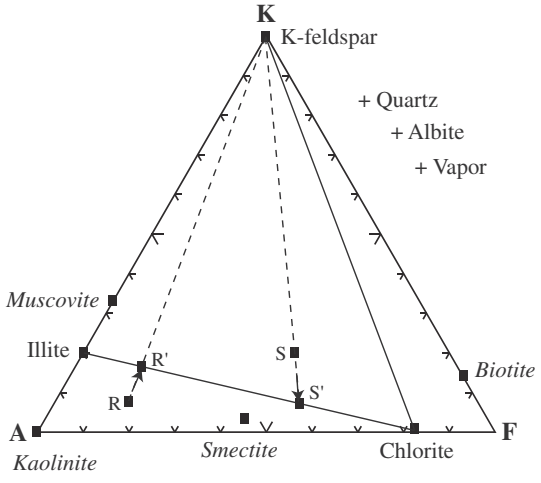

Fig. 5. The AKF diagram. In this type of representation, at equilibrium in a PT range, rock R would contain kaolinite + illite + chlorite + quartz (+albite + vapour) and rock S illite + chlorite + K-feldspar + quartz (+albite + vapour). Due to metasomatism, the composition of rock R has moved to R′ by gaining K and that of rock S to S′ by losing K. Irrespective of the nature of their original clay minerals, all final compositions lie on the illite-chlorite join.

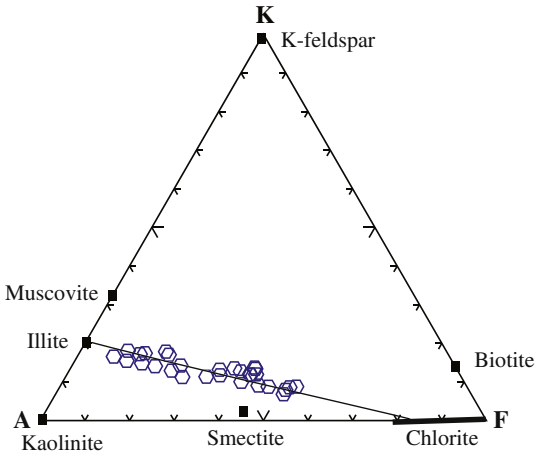

Fig. 6. The rock compositions of the La Roche cross section (Table 2) plotted in the AKF triangle. Irrespective of the formation to which the rocks belong or to their quartz content, all rocks tend to plot on an illite-chlorite tie line.

parameter (Fig. 8a) on average higher than in the younger formations, and showing a large dispersion of values. Low values of the #Mg are also typical of these formations (Fig. 8b). As discussed above, the AAFM parameters can be interpreted as a proxy to the source composition. In the present case, the OSM derive on average from a source richer in aluminium and with a lower Mg/Fe ratio than younger formations. In addition, the younger formations show AAFM and #Mg values similar to the PAAS (Post Archean Australian Shale; Taylor and McLennan, 1985). It thus appears that the OSM source with high values of the AAFM is very unusual.

The distinction between the sources is less marked when other parameters are considered. The Al/Ti ratio (Fig. 8c) oscillates between 10 and 20 around the PAAS value, reflecting the correlation of these elements in the PCA analysis. It is not possible to demonstrate the possible influence of eolian fluxes (Yarincik et al., 2000) or of enhanced delivery of riverine detritus (Murphy et al., 2000). The MnO content is similar in OSM and La Roche with a large increase in the Chooz Formation (Fig. 8d). The Zr concentrations on average are not different between OSM and La Roche, but a large excursion is to be noted in the Pesche Formation (Fig. 8f). The V concentration largely varies throughout the whole column without significant contrast at the OSM/La Roche transition (Fig. 8e). Same remark is valid for the Cr content at the transition (Fig. 8g). There is an overall two-fold decrease of Cr values which might reflects an increase in suboxic conditions (Sageman and Lyons, 2013). In the Pesche Formation, a large Cr value is observed in a Zr rich sample, consistent with the resistate character of both elements.

In conclusion, the best proxies to characterize the change in the source composition is the AAFM and #Mg parameters. In the La Roche profile, a major change occurred at the OSM/La Roche transition and the OSM source ceased to produce detrital material after the Mirwart Formation. This change corresponds moreover to a major pulse in the Devonian transgression: the tidal environment of the Mirwart Formation is followed by shallow sea in the Villé Formation then by deeper sea in the La Roche Formation (Dejonghe and Hance, 2001).

4.6. Regional extension of the OSM/La Roche transition

The regional extension of the AAFM change at the OSM/La Roche transition can be appreciated by considering the chemical compositions of 109 samples collected in the other cross sections (Supplementary Table S3). Average compositions of specific concentrations and ratios from the various formations are displayed in Table 3. A

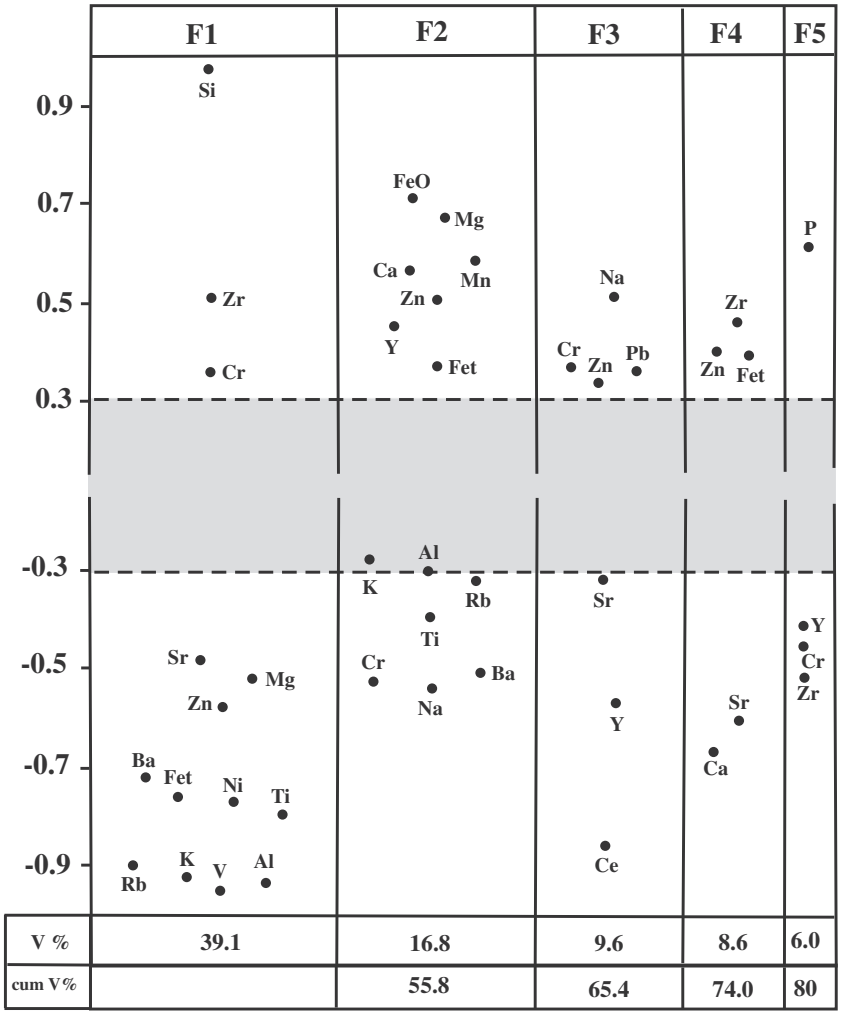

Fig. 7. Graphical representation of the factor loadings of the five principal components. "V%" is the proportion in % of total variance taken by the components, and "cum V%" is the cumulative percentage.

Please cite this article as: Duchesne, J.-C., et al., Geochemistry of Lower Devonian terrigenous sedimentary rocks from the Belgian Ardenne: Source proxy and paleogeographic reconstruction, Sedimentary Geology (2017), https://doi.org/10.1016/j.sedgeo.2017.11.008

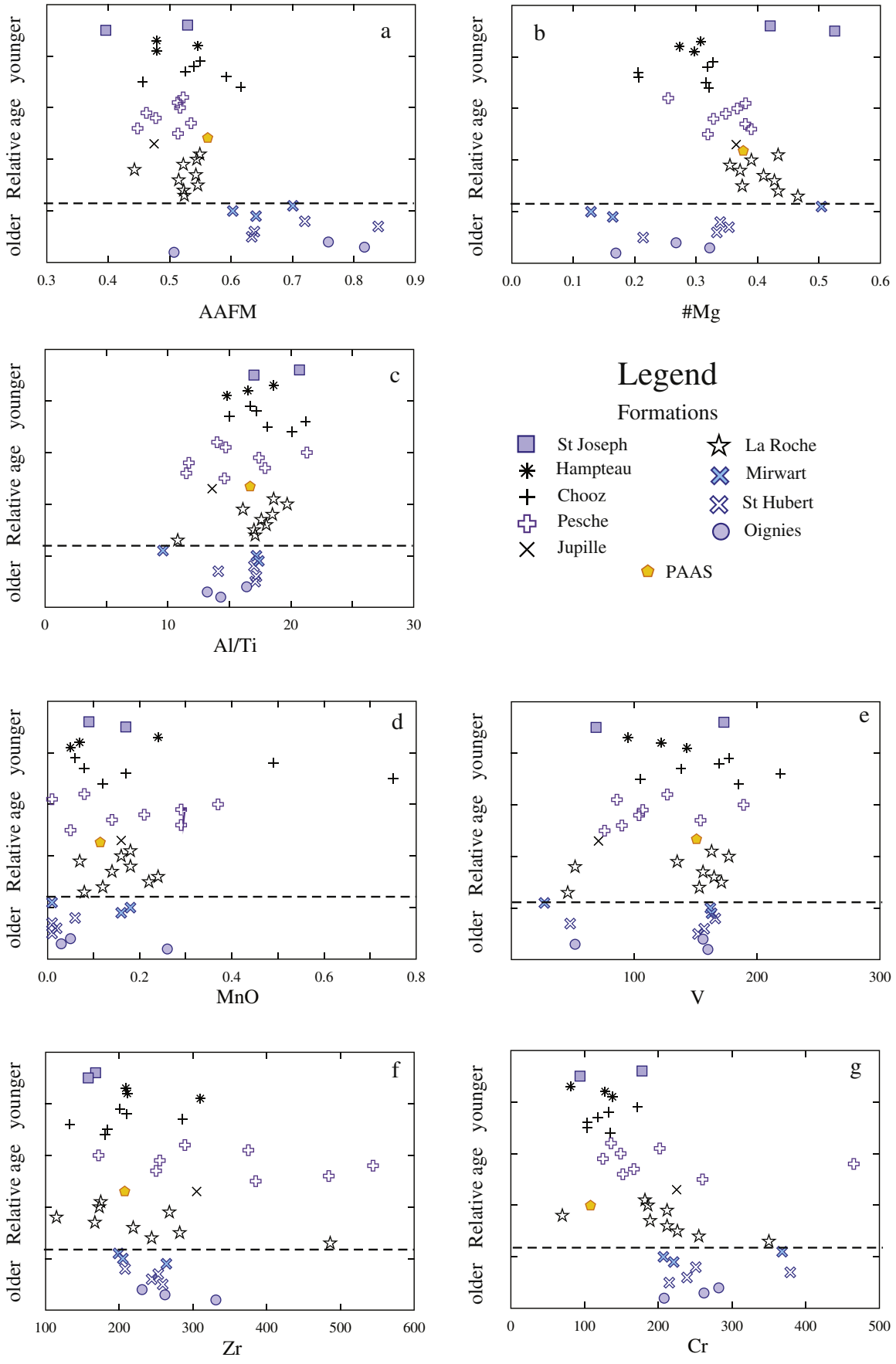

Fig. 8. Stratigraphic evolution of significant parameters in the La Roche cross section. Data from Table 2. PAAS composition after Taylor and McLennan (1985). The horizontal dashed line indicates the limit between the Mirwart and the La Roche Formations.

Please cite this article as: Duchesne, J.-C., et al., Geochemistry of Lower Devonian terrigenous sedimentary rocks from the Belgian Ardenne: Source proxy and paleogeographic reconstruction, Sedimentary Geology (2017), https://doi.org/10.1016/j.sedgeo.2017.11.008

comparison between the 5 cross sections is provided in Figs. 9, 10 and 12, on which the evolution of parameters vs. stratigraphic age in the various formations is shown. It comes that high values of the AAFM parameter and a large dispersion are also observed in the E411 and E25 profiles that are *c.* 30 km to the west and 13 km to the east, respectively, of the La Roche cross section. In the Couvin profile, 50 km west of E411, a high AAFM value is observed in the Mondrepuis Formation, below the Oignies Formation, and values closer to the average characterize the St Hubert and Mirwart Formations. From this distribution of AAFM values it is suggested that the major change occurring after the OSM formations is of regional extension and, hence, that the OSM source has influenced this part of the Ardenne Anticline. In the Hoyoux profile (Fig. 10), the contrast between the various formations is less well marked, with only 2 samples in Nonceveux and one sample in Marteau above average. This suggests that the OSM source had no or not much influence in the northern part of the Dinant Synclinorium.

In the northern part of the Ardenne Anticline, low values of the #Mg ratio are characteristic of the OSM formations in the La Roche, E411 and E25 cross sections (Fig. 9), but when average values by formations are considered (Table 3), the OSM formations are more difficult to distinguish from the younger ones. The same remark holds also for the Hoyoux section (Fig. 10) where #Mg values are within error similar in all younger formations (Table 3). It thus comes that #Mg is a less efficient parameter than AAFM to discriminate the OSM formations from the other ones.

4.7. The Rocroi Massif as the source of the OSM formations

As recalled above, there is strong geological evidence (Meilliez, 1984) that the Rocroi massif was emerged in Lochkovian times, and palynological evidence (Steemans, 1989) that it could have been the source of sediments in the northern part of the Ardenne Anticline. The Rocroi "Island" ceased to exist during most Pragian and Emsian times. Our geochemical data concur with this model. The aluminium-rich OSM formations are of regional extension in the northern part of the Ardenne Anticline and limited to Lochkovian and Early Pragian times. The Rocroi Massif can thus be the source of this aluminium-rich detrital material. Interestingly, the regional distribution of the Zr concentrations in the OSM formations (Fig. 11) supports this interpretation. As shown in Fig. 11a, there is an overall decreasing trend in the average Zr concentrations from the Couvin cross section, proximal to the Rocroi Massif, to the E25 cross section, some 110 km to the E, in a distal position relative to the Rocroi Massif. To account for the possible dilution by quartz, the Zr concentrations have been normalized to an Al_2O_3 content of 15% (Garcia et al., 2004). Here again the overall decrease of the averages is patent from Couvin to E25. Entrainment sorting of heavy minerals in the bed load has thus taken place in the transport from the source to the depositional sites.

The peculiar geochemical characteristics of OSM material possibly result from kaolinitization of acidic rocks or could come from the erosion of alterites similar to those formed from Devonian rocks on the high plateau of the Ardenne (Dumoulin and Blockmans, 2013b). Evidence of pre-Lockhovian acidic magmatism in the Rocroi Massif is provided by clasts of rhyolitic quartz phenocrysts in Lower Devonian sediments at Willerzie (Beugnies, 1968). Moreover, Silurian ages (420.5 ± 2.9 Ma and 421.1 ± 4.0 Ma) have been measured on zircon grains from the Mairupt microgranite dykes (Cobert et al., 2016). Paradoxically, Upper Devonian ages (373 +8/−9 Ma; Goffette et al., 1991) have also been obtained on the Mairupt dyke. It is thus possible that a second intrusive event has taken place in the same dyke system. It should also be noted that the Mid German High, although containing acidic rocks (igneous or metamorphic) likely to generate aluminium-rich detritus, is not a plausible source of the OSM formations. It indeed remained emerged

Table 3
Average composition and standard deviation of specific values from the studied formations.

	North of Ardenne Anticline																North of Dinant Synclinorium											
Formation	Hierg.-Hampt.		Chooz		Villé		Vireux		La Roche		Pesche		Oignies		St Hubert		Mirwart		Marteau		Nonceveux		Solières		Acoz		Wépion	
n	5		10		9		2		17		11		10		14		10		16		21		3		9		2	
		s		s		s		s		s		s		s		s		s		s		s		s		s		s
MnO (%)	0.10	*0.08*	0.22	*0.24*	0.13	*0.09*	0.14	*0.10*	0.12	*0.07*	0.15	*0.12*	0.05	*0.06*	0.03	*0.03*	0.10	*0.09*	0.12	0.16	0.09	0.05	0.08	0.02	0.12	0.09	0.04	0.02
Ba	408	*109*	554	*123*	556	*153*	719	*103*	475	*209*	405	*170*	613	*226*	723	*194*	642	*241*	279	90	620	147	583	62	612	140	597	89
Cr	143	*44*	139	*26*	207	*36*	170	*20*	233	*69*	200	*97*	239	*48*	283	*80*	263	*80*	141	91	203	38	206	42	222	40	165	10
Ni	59	*10*	64	*8*	67	*12*	74	*25*	71	*31*	57	*14*	65	*24*	49	*27*	77	*28*	60	31	84	19	95	19	103	15	79	4
Rb	136	*41*	156	*45*	157	*39*	202	*15*	141	*60*	117	*56*	136	*38*	162	*45*	149	*58*	133	58	156	36	204	20	187	16	177	38
Sr	101	*30*	94	*19*	79	*37*	111	*2*	111	*47*	82	*19*	112	*59*	135	*60*	102	*41*	53	18	60	17	71	13	68	12	90	28
V	146	*40*	168	*32*	158	*24*	187	*11*	145	*53*	131	*45*	136	*34*	150	*33*	155	*45*	101	43	152	29	194	15	183	14	167	27
Y	34	*13*	28	*5*	28	*6*	40	*4*	24	*8*	31	*6*	29	*7*	32	*7*	33	*8*	27	9	23	7	23	5	24	6	28	1
Zn	83	*31*	109	*14*	96	*41*	138	*31*	85	*37*	104	*29*	64	*32*	50	*37*	81	*65*	78	29	105	39	142	8	126	30	110	18
Zr	240	*45*	205	*55*	219	*32*	177	*15*	233	*84*	317	*116*	277	*64*	232	*36*	236	*64*	250	123	243	74	162	4	209	17	244	29
Ce	168	*85*	117	*20*	78	*16*	135	*8*	83	*28*	96	*29*	75	*26*	75	*26*	86	*22*	83	32	96	20	117	16	126	13	112	12
AAFM	0.52	*0.04*	0.54	*0.04*	0.56	*0.04*	0.58	*0.00*	0.54	*0.07*	0.51	*0.05*	0.61	*0.13*	0.73	*0.13*	0.61	*0.17*	0.52	0.08	0.55	0.07	0.56	0.02	0.55	0.04	0.58	0.09
#Mg	0.33	*0.06*	0.28	*0.05*	0.38	*0.06*	0.30	*0.02*	0.41	*0.04*	0.35	*0.04*	0.35	*0.13*	0.30	*0.13*	0.41	*0.16*	0.37	0.09	0.43	0.08	0.40	0.05	0.39	0.06	0.40	0.01
Al/Ti	16.9	*1.4*	17.5	*2.2*	17.8	*1.3*	18.4	*0.4*	16.5	*2.7*	16.0	*3.0*	16.1	*2.1*	17.8	*1.8*	17.9	*2.2*	17.9	7.6	16.4	2.1	18.8	1.6	17.4	0.7	16.5	1.1

n is the number of samples in the formation.

up to the Emsian and thus would have produced aluminium-rich material after the Lochkovian in Pragian times, which is not observed.

4.8. The Stavelot Massif as a temporary source

In the La Roche and E411 cross sections (Fig. 12), the MnO concentrations reach maximum values in the Chooz Formation. This could confirm the suggestion based on geological evidence that the Stavelot massif was emerged in Late-Emsian times and could have provided Mn-rich detritus mixed with more common sediments. The high content of a sample at the top of the Wepion Formation in the Hoyoux cross section is in agreement with this hypothesis but the evidence is rather meagre. The low content in the Chooz Formation in the Couvin area can be explained by the long distance to the source (more than 80 km) (Fig. 1). High values observed in the Hoyoux cross section in the lower part of the Marteau Formation could also be explained by the emersion of the Stavelot Massif at the beginning of the Lochkovian, as explained above. It remains that in the La Roche cross section the 0 to 0.40% MnO range is much higher than the PAAS average (0.11% MnO). This could indicate local more oxidizing conditions favouring precipitation of insoluble Mn-oxyhydroxides (Sageman and Lyons, 2013) in the La Roche basin.

4.9. Local variations of some proxies

It is interesting to appreciate whether variation of some parameters (other than AAFM) in one section has a regional significance. Are, for

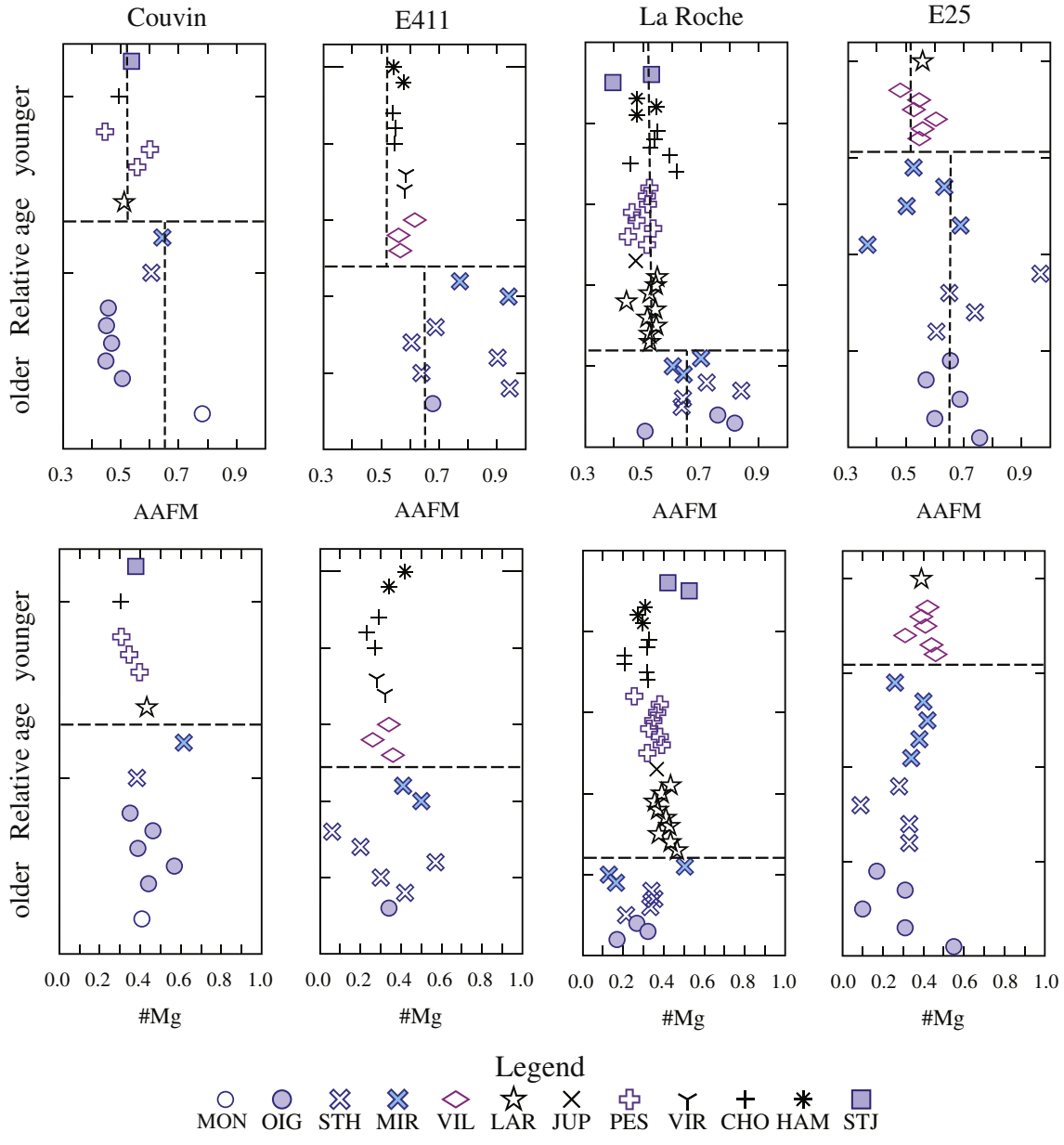

Fig. 9. Comparison of the evolution of the AAFM and #Mg parameters in the 4 profiles coming from the North Ardenne Anticline and East Dinant Syncline. The horizontal dashed line figures the limit between the Mirwart Formation and younger formations (La Roche or Villé). The vertical dashed lines give the average value of the AAFM parameter (Table 3) in all samples belonging to the OSM and Mondrepuis Formations and in those younger than the Mirwart Formation. Note that the AAFM values are not only higher on average in the OSM formations but also more dispersed than in the younger formations. Legend: Formation abbreviations as in Fig. 3.

Please cite this article as: Duchesne, J.-C., et al., Geochemistry of Lower Devonian terrigenous sedimentary rocks from the Belgian Ardenne: Source proxy and paleogeographic reconstruction, Sedimentary Geology (2017), https://doi.org/10.1016/j.sedgeo.2017.11.008

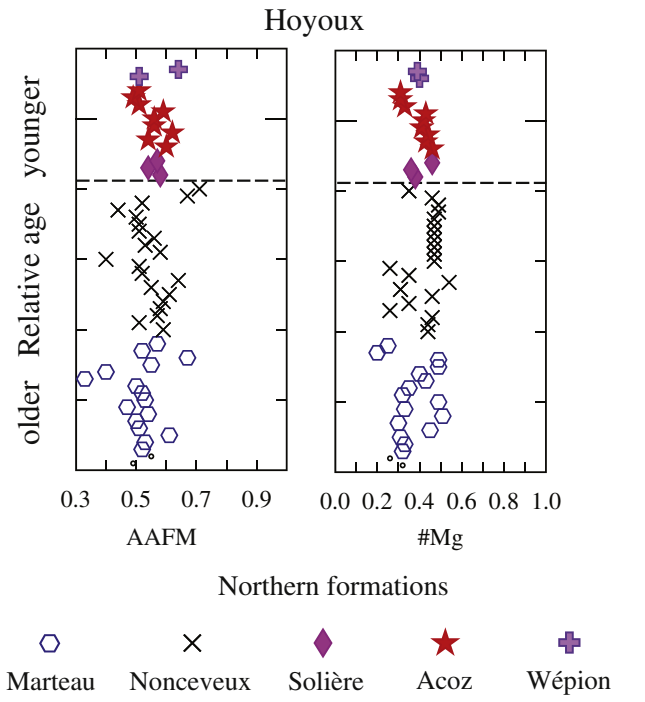

Fig. 10. Evolution of the AAFM and #Mg parameters in the Hoyoux cross section (northern part of the Dinant Synclinorium). The horizontal line is between the Nonceveux and Solières Formations, at approximately the same age as in the southern cross sections.

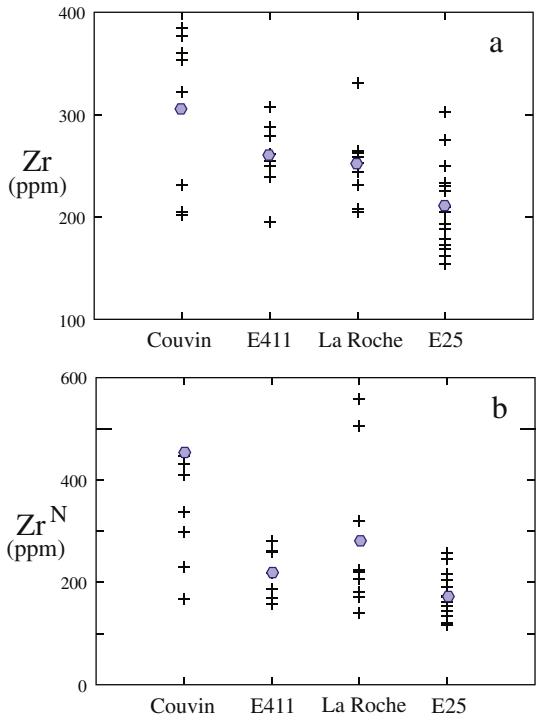

Fig. 11. Zr concentrations (in a) and Zr normalized values to 15% Al_2O_3 (i.e. Zr^N = Zr (ppm) * 15/Al_2O_3 (%)) (in b) in the samples from the OSM formations in the four cross sections. Legend: cross: values from Table 2 and S3; filled symbol: average values. Note that in b a very high value (1303 ppm) in sample C11 in the Couvin cross section is not represented but has been taken into account in the average.

instance, the high values of Zr in the Pesche Formation or at the base of the La Roche Formation occurring in the La Roche cross section (Fig. 8f) also observed in the other cross sections? It is not the case, which means that this character is not related to a change in the source but to local sorting processes. Same question for the low Al/Ti ratios at the transition between the Mirwart and the La Roche Formations (Fig. 8c) that are not observed in the other cross sections. This is too local to be due to a regional variation in the relative fluxes of weathered riverine or eolian fractions to bulk sedimentation. These somewhat chaotic variations of parameters at the regional scale are very likely related to the deltaic environment of the Lower Devonian in the Ardenne. A lack of regional homogeneity would result from the multiplicity of streams, each with particular terrigenous sediment load, meandering and interacting in the alluvial plain, as well as from a variety of local depositional modes and redox conditions.

5. Conclusions

The major element composition of the terrigenous sediments projected in the AKF diagram reveals that all rocks, whatever their quartz contents, plot on the illite-chlorite tie line. This paragenesis thus results from the reaction of the detrital clay minerals with potassium in postdepositional processes and this confirms that the chemical system has reached equilibrium in open system conditions. The change in the original composition of the detrital material was not sufficient to significantly alter the characteristics of the source material and the final illite/chlorite ratio of the rock mirrors the aluminium to iron plus magnesium ratio in the source material. This permits the definition of the AAFM proxy.

Statistically, the behaviour of Ti, V and partly Cr in postdepositional processes appear linked to illite neoformation and part of Cr to resistate minerals. The use of Ti/Al as a proxy of detritus source and of Cr and V as proxies of redox conditions must thus be taken with caution.

In the La Roche cross section, the evolution of the AAFM proxy shows a major change at the limit between the Mirwart and the La Roche Formation. This is interpreted as a shift from a source producing aluminium-rich clay minerals such as kaolinite or detrital illite to a source generating more common clay minerals such as smectite and detrital chlorite.

This major change between the Mirwart Formation and younger formations is also observed in the Couvin, E411 and E9 cross sections but not in the Hoyoux cross section. It can thus be concluded that it characterizes the paleogeography of the northern part of the Ardenne Anticline but not the northern part of the Dinant Synclinorium. The most plausible source of the aluminium-rich material is the Rocroi Massif that was emerged in Lochkovian times and has supplied detritus in the northern regions of the Ardenne Anticline but did not reach the Hoyoux cross section in the northern part of the Dinant Synclinorium. This conclusion in good agreement with a previous suggestion based of palynological data (Steemans, 1989). There is some evidence that Mn-rich sediments occur in the Chooz Formation, which could indicate that the Stavelot Massif has emerged in Emsian times, but this conclusion needs further support.

Supplementary data to this article can be found online at https://doi.org/10.1016/j.sedgeo.2017.11.008.

Acknowledgments

Sébastien Bertrand, Bernard Charlier, Eric Goemaere, Léon Dejonghe, Edith Wilmart, Jacques Bellière and the late Georges Vandenven are particularly thanked for their help at various stages of this research. This research was supported by the Belgian Fund for Basic Collective Research (programme no. 112). Tomáš Kumpan, an anonymous reviewer and the editors of this book are greatly thanked for their constructive suggestions.

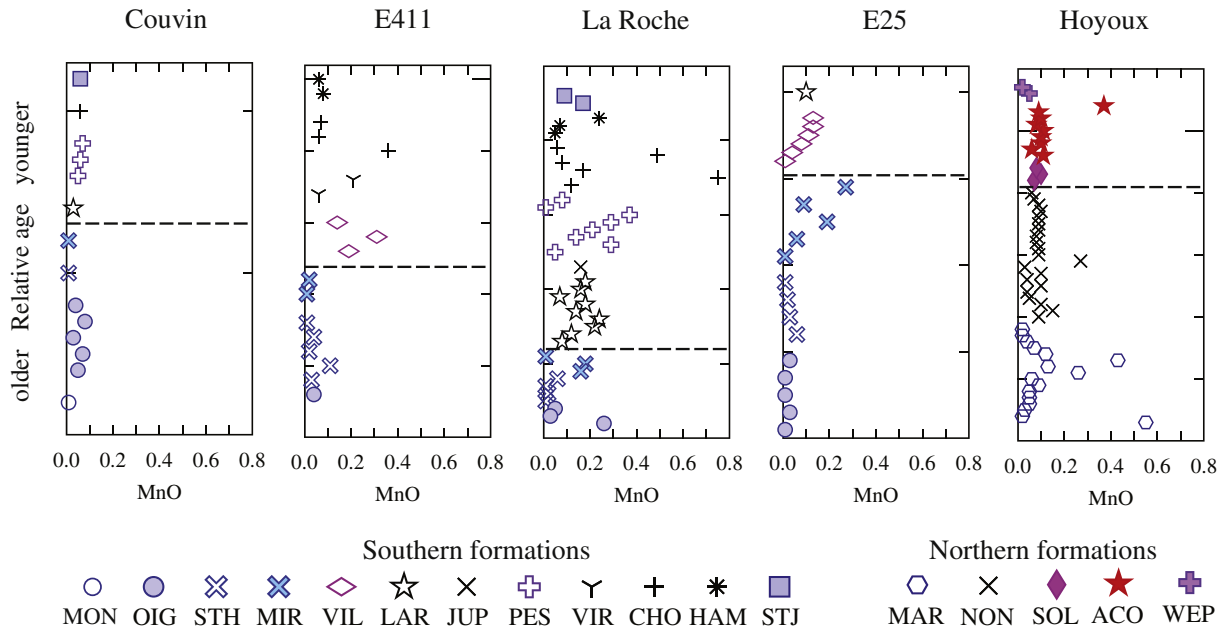

Fig. 12. Evolution of the MnO contents in the five cross sections. Same legend as in Figs. 9 and 10. Formation abbreviations as in Fig. 3.

References

Beugnies, A., 1968. Les roches à quartz dihexaédriques du Franc-Bois de Willerzie. Bulletin Société belge de Géologie 77, 311–329.

Beugnies, A., 1986. Le métamorphisme de l'aire anticlinale de l'Ardenne. Hercynica 2, 17–33.

Bologne, G., Duchesne, J.C., 1991. Analyse des roches silicatées par spectrométrie de fluorescence X: précision et exactitude. Belgian Geological Survey Professional Paper 249, 1–11.

Bossiroy, D., 1984. Contribution à l'étude pétrographique des roches métamorphiques du Massif de Stavelot. Licence thesis. Department of Geology, University of Liege, Liege.

Boulvain, F., Pingot, J.-L., 2016. Une introduction à la Géologie de la Wallonie. http://www2.ulg.ac.be/geolsed/geolwal/geolwal.htm Department of Geology, University of Liege.

Boulvain, F., Vandenberghe, N., 2017. An introduction to the geology of Belgium and Luxembourg. In: Demoulin, A. (Ed.), Landscapes and Landforms of Belgium and Luxembourg. Springer, pp. 9–33.

Bucher, K., Frey, M., 1994. Petrogenesis of Metamorphic Rocks. Springer, Heidelberg.

Bultynck, P., Dejonghe, L., 2001. Devonian lithostratigraphic units (Belgium). In: Bultinck, P., Dejonghe, L. (Eds.), Guide to a Revised Lithostratigraphic Scale of Belgium. Geologica Belgica 4, pp. 39–69.

Bultynck, P., Coen-Aubert, M., Dejonghe, L., Godefroid, J., Hance, L., Lacroix, D., Preat, A., Stainier, P., Steemans, P., Streel, M., Tourneur, F., 1991. Les formations du Dévonien moyen de la Belgique. Mémoires pour Explication Cartes Géologiques et Minières Belgique 30 106 pp.

Chamley, H., 1989. Clay Sedimentology. Springer, Heidelberg.

Cobert, C., Baele, J.-M., Boulvais, P., Poujol, M., Beyssac, O., Decrée, S., 2016. Upper Silurian magmatism in the Rocroi Massif, Ardennes: new constraints from geochronology of microgranite at Mairupt (abstract). 5th International Geologica Belgica Meeting, University of Mons.

Colbeaux, J.P., Beugnies, A., Dupuis, C., Robaszinsky, F., Somme, J., 1977. Tectonique de blocs dans le sud de la Belgique et le nord de la France. Annales Société géologique du Nord 97, 191–222.

Dejonghe, L., 2008. Carte géologique de la Wallonie, Hotton - Dochamps 55/5–6, 1/25000. Ministère de la Région Wallonne, Direction Générale des Ressources Naturelles et de l'Environnement.

Dejonghe, L., Hance, L., 2001. Carte géologique de Wallonie, Champlon - La Roche-en-Ardenne 60/1–2, 1/25000. Ministère de la Région Wallonne, Direction Générale des Ressources Naturelles et de l'Environnement.

Dumoulin, V., Blockmans, S., 2013a. Carte géologique de Wallonie, Felenne - Vencimont 58/7–8, 1/25000. Ministère de la Région Wallonne, Direction Générale des Ressources Naturelles et de l'Environnement.

Dumoulin, V., Blockmans, S., 2013b. Carte géologique de Wallonie, Pondrôme - Wellin 59/5–6, 1/25000. Ministère de la Région Wallonne, Direction Générale des Ressources Naturelles et de l'Environnement.

Eskola, P., 1920. The mineral facies of rocks. Norsk Geologisk Tidsskrift 6, 143–194.

Fielitz, W., Mansy, J.L., 1999. Pre- and synorogenic burial metamorphism in the Ardenne and neighbouring areas (Rhenohercynian zone, central European Variscides). Tectonophysics 309, 227–256.

Fourmarier, P., 1931. Les plissements calédoniens et les plissements hercyniens en Belgique. Annales Société géologique de Belgique 54, B364–384.

Franke, W., 2000. The mid-European segment of the Variscides: tectonostratigraphic units, terrane boundaries and plate tectonic evolution. In: Franke, W., Haack, V., Oncken, O., Tanner, D. (Eds.), Orogenic Processes, Quantification and Modelling in the Variscan Belt. Geological Society of Londo, Special Publications Vol. 179, pp. 35–61.

Garcia, D., Ravenne, C., Maréchal, B., Moutte, J., 2004. Geochemical variability induced by entrainment sorting: quantified signals for provenance analysis. Sedimentary Geology 171, 113–128.

Godefroid, J., Blieck, A., Bultynck, P., Dejonghe, L., Gerrienne, P., Hance, L., Meilliez, F., Stainier, P., Steemans, P., 1994. Les formations du Dévonien inférieur du Massif de la Vesdre, de la Fenêtre de Theux et du Synclinorium de Dinant (Belgique, France). Mémoires pour Explication Cartes Géologiques et Minières de la Belgique 38, 1–144.

Goemaere, E., Dejonghe, L., 2005. Paleoenvironmental reconstruction of the Mirwart Formation (Pragian) in the Lambert Quarry (Flamierge, Ardenne, Belgium). Geologica Belgica 8, 37–52.

Goffette, O., Liégeois, J.-P., André, L., 1991. Age U-Pb sur zircon dévonien moyen à supérieur du magmatisme bimodal du massif de Rocroi (Ardenne, France): implications géodynamiques. Comptes Rendus Académie Sciences Paris 312 (série II), 1155–1161.

Herron, M.M., 1988. Geochemical classification of terrigenous sands and shales from core or log data. Journal of Sedimentary Petrology 58, 820–829.

Hower, J., Eslinger, E., Hower, M., Perry, E., 1976. Mechanism of burial metamorphism of argillaceous sediment: 1. Mineralogical and chemical evidence. Geologica Societry of America Bulletin 87, 725–737.

Kramm, U., 1973. Chloritoid stability in manganese rich low-grade metamorphic rocks, Venn-Stavelot Massif, Ardennes. Contributions to Mineralogy and Petrology 41, 179–196.

Kramm, U., 1976. The coticule rocks (spessartine quartzites) of the Venn-Stavelot Massif, Ardennes, a volcanoclastic metasediment? Contributions to Mineralogy and Petrology 56, 135–155.

Marion, J.-M., Barchy, L., 1999. Carte géologique de Wallonie, Chimay - Couvin, 57/7–8, 1/25000. Ministère de la région Wallonne, Direction Générale des Ressources Naturelles et de l'Environnement.

Meilliez, F., 1984. La Formation de Fépin (Gédinnien de l'Ardenne): un marqueur régional lithostratigraphique et structural. Annales Société géologique du Nord 53, 37–53.

Meus, P., 1984. Etude pétrographique et géochimique du Dévonien inférieur à Laroche et Couvin. Licence thesis. Department of Geology, University of Liege, Liege.

Milliken, K., 2013. In: MacKenzie, F.T. (Ed.), Late diagenesis and mass transfer in sandstone-shale sequences, second editionSediments, Diagenesis, and Sedimentary Rocks: Treatise on Geochemistry 7, pp. 159–190.

Murphy, A.E., Sageman, B.B., Hollander, D.J., Lyons, T.W., Brett, C.E., 2000. Black shale deposition in the devonian Appalachian Basin: siliciclastic starvation, episodic water-column mixing, and efficient recycling of biolimilting nutrients. Paleoceanography 15, 280–291.

Norrish, K., Hutton, J.T., 1969. An accurate X-ray spectrographic method for the analysis of a wide range of geological samples. Geochimica et Cosmochimica Acta 33, 431–453.

Ohr, M., Halliday, A., Peacor, D., 1994. Mobility and fractionation of rare earth elements in argillaceous sediments: implications for dating diagenesis and low-grade metamorphism. Geochimica et Cosmochimica Acta 58, 289–312.

Roelandts, I., Duchesne, J.C., 1988. AW-1, SBO-1, PRI-1, CCH-1 and DWA-1, Belgian sedimentary sock reference materials. Geostandards Newsletter 12, 13–18.

Please cite this article as: Duchesne, J.-C., et al., Geochemistry of Lower Devonian terrigenous sedimentary rocks from the Belgian Ardenne: Source proxy and paleogeographic reconstruction, Sedimentary Geology (2017), https://doi.org/10.1016/j.sedgeo.2017.11.008

Roelandts, I., Duchesne, J.C., 1994. 1993 compilation of data on five Belgian sedimentary rock reference materials: AWI-1, SBO-1, PRI-1, CCH-1 and DWA-1. Geostandards Newsletter 18, 143–184.
Sageman, B.B., Lyons, T.W., 2013. In: MacKenzie, F.T. (Ed.), Geochemistry of fine-grained sediments and sedimentary rocks, second editionSediments, Diagenesis, and Sedimentary Rocks: Treatise on Geochemistry 7, pp. 115–158.
Steemans, P., 1989. Paléogéographie de l'Eodévonien ardennais et des régions limitrophes. Annales Société géologique de Belgique 112, 103–119.
Stets, J., Schäfer, A., 2002. Depositional environments in the Lower Devonian siliciclastics of the Rhenohercynian Basin (Rheinische Schiefergebirge, W-German): case studies and a model. Contributions to Sedimentary Geology 22.
Stets, J., Schäfer, A., 2009. The Siegenian delta: land-sea transitions at the northern margin of the Rhenohercynian Basin. Geological Society of London, Special Publication 314, 37–72.
Taylor, S., McLennan, S., 1985. The Continental Crust: Its Composition and Evolution. Blackwell, Oxford.
Turner, F.J., Verhoogen, J., 1960. Igneous and Metamorphic Petrology. McGraw-Hill Book Company, Inc., New York.
Velde, B., 1983. Diagenetic reactions in clays. In: Parker, A., Sellwood, B.W. (Eds.), Sediment Diagenesis. Reidel, Dordrecht, pp. 215–268.
Verhoogen, J., Turner, F.J., Weiss, L.E., Wahrhaftig, C., Fyfe, W.S., 1970. The Earth, an Introduction to Physical Geology. Holt, Rinehart and Winston, Inc., New York.
Wilmart, E., Baudelet, M., Bologne, J., Schoumacher, C., Bellière, J., Duchesne, J.C., 1984. Modèle géochimique des sédiments paléozoïques du sud de la Belgique. Méthodologie pour l'étude des matériaux pélitiques., Fonds de la Recherche Fondamentale Collective, Programme d'initiative ministérielle n°112, Department of Geology, University of Liege 325 pp.
Winkler, H.G.F., 1979. Petrogenesis of Metamorphic Rocks. Springer, Heidelberg.
Winter, J., 2001. An Introduction to Igneous and Metamorphic Petrology. Prentice Hall, Upper Saddle River.
Yarincik, K.M., Murray, R.W., Petreson, L.C., 2000. Climatically sensitive eolian and hemipelagic deposition in the Cariaco Basin, Venezuela, over the past 578,000 years: results from Al/Ti and K/Al. Paleoceanography 15, 210–228.
Ziegler, P.A., 1990. Geological Atlas of Western and Central Europe. 2nd ed. Shell Internationale Petroleum Maatschappij BV, Den Haag.

Please cite this article as: Duchesne, J.-C., et al., Geochemistry of Lower Devonian terrigenous sedimentary rocks from the Belgian Ardenne: Source proxy and paleogeographic reconstruction, Sedimentary Geology (2017), https://doi.org/10.1016/j.sedgeo.2017.11.008